Mapping the Range of Simple Fresh Lunar Crater Ejecta by Analyzing the Scattering Characteristics of the Lunar Regolith Using Mini-RF Data

Zhaobo Song, Zhanchi Huang, Gaofeng Shu, *Member, IEEE*, Zhengwei Guo, and Ning Li, *Member, IEEE*

***Abstract*— Lunar crater ejecta can provide important information regarding the impact cratering process and the properties of subsurface materials. However, the mapping of the range of the crater ejecta has been hampered by the degradation of the lunar surface's morphological features. Polarimetric synthetic aperture radar (SAR) is an effective technique to determine the scattering characteristics of the lunar surface and subsurface, and for distinguishing the fresh crater ejecta from surrounding regions. This letter uses a three-component compact decomposition to process the mini-radio frequency (Mini-RF) data to identify the scattering characteristics of the crater floor, crater wall, crater ejecta of the simple fresh crater, and lunar background regolith. Then, a method for mapping the range of crater ejecta is proposed to obtain the boundary between the crater ejecta and other regions by analyzing the differences in polarimetric scattering characteristics. Using this method, the crater ejecta of six craters were extracted and verified with the range of the ejecta obtained through visual interpretation on SAR imagery, the accuracy of the ejecta range obtained by the proposed method is 82%–95%. The results show that the proposed method can effectively depict the range of the simple fresh lunar crater ejecta.**

***Index Terms*— Crater ejecta, lunar crater, lunar regolith, mini-radio frequency (Mini-RF).**

I. Introduction

IMPACT cratering process is the most general geologic process on the lunar surface, and the crater and crater ejecta are the dominant geomorphologic features of the lunar surface [1]. During the crater's formation, the excavation of subsurface materials produces ejecta. More than 90% of the ejecta is deposited near the crater and is called proximal ejecta, which contains a large amount of blocky ejecta and forms an ejecta blanket. The remaining part is composed of fine particles called distal ejecta, which is often deposited only a few centimeters thick and sparsely distributed [2]. The severe erosion of the crater ejecta by micrometeorite impacts, solar wind, and cosmic rays, causes the degradation of the surface morphology of the ejecta deposits, making it difficult to distinguish from the lunar background regolith [3]. The crater ejecta deposits can provide a wealth of information about the impact process and the subsurface materials of the lunar regolith. Therefore, studying the crater ejecta occupies an essential position in lunar exploration.

Optical imagery is an essential data source for characterizing the lunar surface morphology. Many studies have been done on crater identification methods based on optical imagery [4], [5]. However, the optical imagery is limited to characterizing the surface information of the lunar regolith. The degradation of the regolith surface causes optical imagery unable to accurately extract the boundary between the crater ejecta and the lunar background regolith. The mini-radio frequency (Mini-RF) instrument on the lunar reconnaissance orbiter (LRO) spacecraft is a hybrid dual-polarized synthetic aperture radar (SAR) with two wavelengths operating in the S-band and X-band (12.6 and 4.2 cm, respectively), which transmits circularly polarized electromagnetic (EM) waves and coherently receives two orthogonal linearly polarized EM waves [6], [7]. Based on the penetration and polarization characteristics of radar EM waves, the subsurface characteristics of the lunar can be detected by analyzing radar backscattering echoes, reducing the influence of the degradation of the lunar surface, and accurately extracting the range of the crater ejecta. However, unlike fresh craters, for degraded craters with highly degraded surface and subsurface features, the characteristics of the block ejecta within the radar detectable range (about 1 m below the lunar surface) have also degraded. Therefore, this letter mainly studies fresh craters.

This study aims to extract the boundary between the simple fresh lunar crater ejecta and surrounding regions using Mini-RF data. The radius of a simple crater is less than 15 km, the crater floor is flat, and there is no central peak [1]. The polarization decomposition of radar echo data differentiates fully polarized and randomly polarized constituents, representing deterministic scattering processes (single bounce scattering and double bounce scattering) and volume scattering processes, respectively [8]. The lunar background regolith can be characterized as predominately single bounce scattering. The crater interior and crater ejecta are characterized by a combination of double bounce and volume scattering due to the higher roughness caused by the relatively high fraction of centimeter- to meter-scale scatterers [8]. The boundary between the crater ejecta and surrounding regions is extracted by analyzing the scattering characteristics in different regions, and the results will be verified with the range of the ejecta obtained through visual interpretation on SAR imagery.

The rest of this letter is organized as follows: Section II introduces the study area and the data. Section III introduces

Manuscript received 30 October 2023; revised 11 January 2024; accepted 17 January 2024. Date of publication 19 January 2024; date of current version 1 February 2024. This work was supported by the Natural Science Foundation of Henan under Grant 222300420115. *(Corresponding author: Gaofeng Shu.)*

The authors are with the College of Computer and Information Engineering, the Henan Key Laboratory of Big Data Analysis and Processing, and the Henan Province Engineering Research Center of Spatial Information Processing, Henan University, Kaifeng 475004, China (e-mail: gaofeng.shu@henu.edu.cn).

Digital Object Identifier 10.1109/LGRS.2024.3356201

TABLE I
STUDY AREA

Index	Name	Longitude	Latitude	Radius/km
1	Crater1	21.0°E	64.3°N	0.50
2	Crater2	23.1°W	48.3°N	0.70
3	Lassell D	10.5°W	14.5°S	1.05
4	Linne	11.8°E	27.7°N	1.20
5	Herigonius K	36.4°W	12.8°S	1.45
6	Condamine S	25.2°W	57.3°N	1.95

the method for extracting the region of the crater ejecta. In Section IV, the proposed method was used to map the range of the crater ejecta of one of the craters of the study areas, and the results of the range of the crater ejecta of six craters were compared and verified with the range of the ejecta obtained through visual interpretation on SAR imagery. Finally, Section V draws the conclusion.

II. STUDY AREA AND DATA

A. Study Area

This study selected six simple fresh craters and their surrounding regions as the study area, and the relevant information is shown in Table I. The radius of the crater is measured through optical imagery. The distinction between fresh and old craters in this letter is based on the observation of clear ejecta traces on SAR imagery. Since the Mini-RF data did not completely cover the surface of the Moon, the selected craters have a radius between 0.5 and 2 km to ensure the completeness of the data.

B. Data

This study has used the Mini-RF data acquired in S-Band zoom mode, which acquires radar images of the lunar surface at 15 × 30 m resolution. Four Stokes parameters are written as

$$I = \begin{bmatrix} I_1 \\ I_2 \\ I_3 \\ I_4 \end{bmatrix} = \begin{bmatrix} \langle |E_{HL}|^2 + |E_{VL}|^2 \rangle \\ \langle |E_{HL}|^2 - |E_{VL}|^2 \rangle \\ 2\mathrm{Re}\langle E_{HL} E_{VL}{}^* \rangle \\ -2\mathrm{Im}\langle E_{HL} E_{VL}{}^* \rangle \end{bmatrix} \quad (1)$$

where I_1 is the total power of the signal, I_2 and I_3 measure the linearly polarized power, and I_4 provides information about the magnitude and sense (left or right) of the circularly polarized power [9].

The degree of polarization (m) has been recognized as the single most important parameter characteristic of a partially polarized EM field [7]. It is defined as

$$m = \frac{\sqrt{I_2^2 + I_3^2 + I_4^2}}{I_1}. \quad (2)$$

Cloude et al. [10] proposed a special three-component compact decomposition, which considers the volume scattering process as the completely unpolarized state. The component representing the volume scattering process can be defined as

$$m_v = \frac{I_1(1-m)}{2}. \quad (3)$$

In the crater ejecta region, volume scattering is the dominant scattering mechanism due to the complex terrain caused by a large amount of blocky ejecta. In this letter, the range of the crater ejecta is characterized by analyzing the component m_v representing the volume scattering process obtained from the three-component compact decomposition.

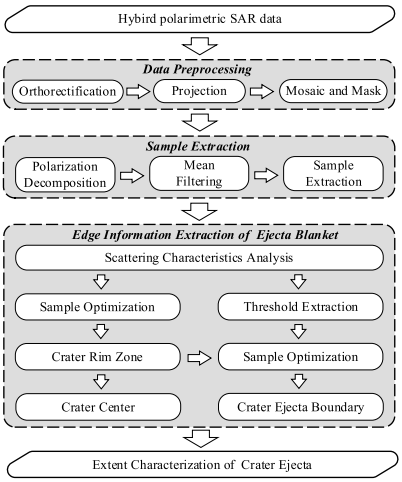

Fig. 1. Flowchart of characterizing the range of crater ejecta.

III. PROPOSED APPROACH FOR MAPPING THE RANGE OF EJECTA BLANKET

Based on Mini-RF data, a complete process to map the range of crater ejecta is proposed. Fig. 1 shows the process of the proposed method.

A. Data Preprocessing

In this letter, the integrated software for imagers and spectrometers (ISISs) [11] and ArcGIS are used to preprocess Mini-RF data. The specific operations are shown in Fig. 1. Orthorectification and projection are used to adjust the geographic information of the data used, and mosaic and mask are used to obtain the specific study area. These operations will not affect the value and resolution of the data.

B. Sample Extraction

The roughness is an important factor affecting the scattering characteristics of the lunar surface [12]. The high roughness of the surface and subsurface of the crater ejecta is caused by the deposition of a large amount of blocky ejecta, making volume scattering the dominant scattering mechanism in the crater ejecta. The deposition of fine particles makes surface scattering the dominant scattering mechanism in the lunar background regolith. This letter uses the component m_v representing the volume scattering process in the three-component compact decomposition to indicate the differences of scattering characteristics in different lunar regions. Fig. 2(a) shows the schematic m_v profile as a function of distance from the crater interior, following the direction of the ejecta flow [13].

A 3 × 3 mean filter is utilized in processing the m_v image to suppress the coherent speckle noise in SAR images. Fig. 2(b) shows the sampling pattern. Set the number of samples to k. A polar coordinate system can be established within the study area with any position on the region located in the center of the crater floor as the pole, and the pole can be used as the first sample point. Starting from the pole and extracting samples outward, each sample should contain all the pixels in the study area in that direction. The radian difference between two

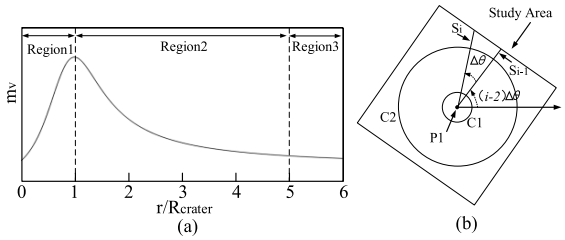

Fig. 2. (a) Schematic m_v profile as a function of distance from the crater interior. r is the distance outward from crater center, while R_{crater} represents the radius of the crater of interest. Region1, Region2, and Region3 represent the crater interior, the crater ejecta, and the lunar background regolith, respectively. (b) Sampling pattern in an m_v image. P1 is the selected pole. C1 and C2, respectively, represent the crater rim and the boundary of the crater ejecta. $\Delta\theta$ represents the angular difference between adjacent samples, S_i and S_{i-1} are two adjacent samples, $i = 1, 2, \ldots, k$.

adjacent samples is related to the set number of samples and the angular difference between adjacent samples $\Delta\theta = 2\pi/k$. The variation in the data of the samples follows the trend shown in Fig. 2(a), and the samples should include information on the crater floor, the crater wall, the crater ejecta, and the lunar background regolith.

C. Edge Information Extraction of Crater Ejecta

Due to the influence of the complex terrain on the lunar surface, the distribution of scattering characteristics in the study area often does not fully conform to the pattern shown in Fig. 2(a). As shown in Fig. 2(a), m_v should reach its maximum value at the crater rim zone and tends to be level off at the boundary between the crater ejecta and the lunar background regolith. This letter used appropriate functions to fit the trend of data variation in the samples in pieces to reduce the influence of complex terrain on the characterization of the crater ejecta.

1) Extraction of the Crater Rim: The coverage area of the crater ejecta starts from the crater rim. As shown in Fig. 2(a), when $r/R_{\text{crater}} \in [0, 2]$, m_v can be fit with a Gaussian function as

$$f_c(x) = \alpha_1 \times \exp\left(-\left(\frac{x-\beta_1}{\gamma_1}\right)^2\right) + \alpha_2 \times \exp\left(-\left(\frac{x-\beta_2}{\gamma_2}\right)^2\right) \quad (4)$$

where $f_c(x)$ represents the value of m_v within the study area when extracting the crater rim. α_1, β_1, γ_1, α_2, β_2, and γ_2 are constants. x is the distance outward from the first sample point, in meters, and $0 \le x \le 2 \times R_{\text{crater}}$.

m_v reaches its maximum value at the crater rim. It can be known through (4) that the distance from the crater rim to the first sample point in the sample can be obtained as

$$l_i = \max_{0 \le x \le 2 \times R_{\text{crater}}} f_c(x). \quad (5)$$

It can be obtained that the coverage range of the crater ejecta in the sample starts from l_i through (5). Using the same method, the positions of the crater rims in all samples can be calculated. Given the coordinates of the first sampling point and the distance l_i from the crater rim to the first sampling point in the nth sample, the coordinates of the crater rim can be obtained using the Pythagorean theorem. By calculating the average value of the coordinates of the crater rim in all samples, the coordinates of the crater center can be obtained.

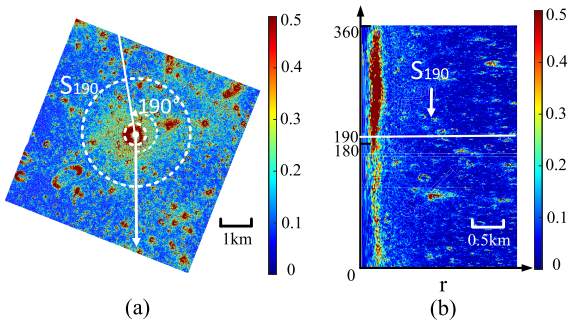

Fig. 3. Crater2 (a) establishment of polar coordinates in m_v image. S_{190} is the sample extracted at a sampling angle of 190° and (b) set of all samples extracted in (a).

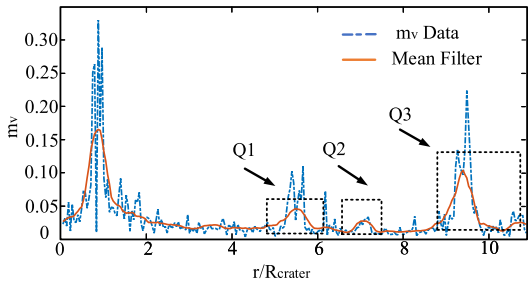

Fig. 4. m_v data and the data after mean filtering of S_{190}. Q1, Q2, and Q3 represent the abnormal fluctuations of data in S_{190}. r is the distance outward from the first sample point, while R_{crater} represents the radius of Crater2.

Then, the average value of the distance from the crater rim to the crater center is calculated as the radius of the crater.

2) Extraction of the Boundary of Crater Ejecta: In Fig. 2(b), when $r/R_{\text{crater}} \ge l_i/R_{\text{crater}}$, m_v can be fit with a power function as

$$f_e(x) = \tau \times x^{\varphi} + \omega \quad (6)$$

where $f_e(x)$ represents the value of m_v on the crater ejecta and lunar background regolith. τ, φ, and ω are constants. x is the distance outward from the crater rim, in meters, and $x \ge 0$.

m_v begins to level off at the boundary between the crater ejecta and the lunar background regolith, indicating that the lunar background level of m_v accounts for the largest proportion in the sample. Therefore, in the curve fit for the crater ejecta and the lunar background regolith, the lunar background level of m_v can be used as a threshold to distinguish between the two regions.

The probability density function of all the data can be expressed as

$$f_{\text{pdf}}(x) = \frac{\text{dF}(x, S_i)}{ndx} \quad (7)$$

where S_i represents the ith sample, $F(x, S_i)$ represents the number of values in S_i that are less than x, and n represents the total amount of data in S_i.

Then, the lunar background level of m_v can be expressed as

$$t_i = \arg\max\left\{f_{\text{pdf}}(x)\right\}. \quad (8)$$

However, some small craters distributed on the range of crater ejecta affect the distribution of scattering characteristics on the crater ejecta, causing abnormal fluctuations of the m_v data, which causes the fit result to be biased toward larger values. To reduce the influence of the fluctuations, after fitting the data using (6), define the range in the data that is greater

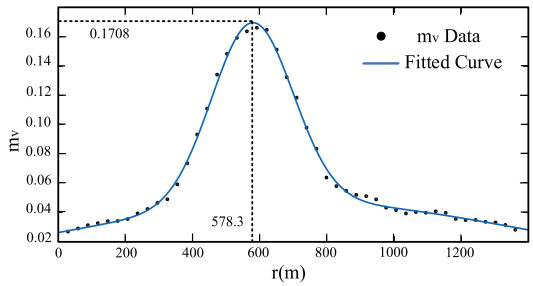

Fig. 5. Data within the research scope and the fitting results when extracting the crater rim is the distance outward from the first sample point, in meters.

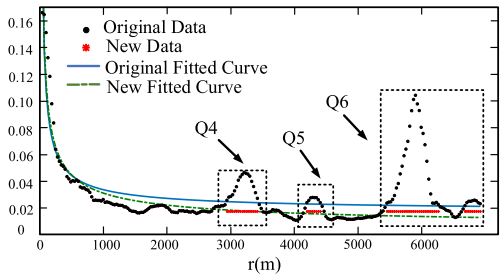

Fig. 6. Data within the research scope and the fitting results when extracting the boundary of the crater ejecta. Q4, Q5, and Q6 correspond to Q1, Q2, and Q3 in Fig. 4, respectively. The black dots represent the original data, and the blue line is its fit curve. The red asterisk is the results after the suppression of abnormal data, and the green line is the fitting result without abnormal data.

than the results of the initial fitting as an anomaly area, and the data in the anomaly area are suppressed to the lunar background level. Then, the data with abnormal fluctuations removed are refitted using (6). The new fit curve conforms to the trend of the data in the sample.

The distance from the first sample point to the boundary between the crater ejecta and the lunar background regolith of the ith sample data can be obtained through (5), (6), and (8) as

$$L_i = \left(\frac{t_i - \omega}{\tau}\right)^{\frac{1}{\varphi}} + l_i. \tag{9}$$

The calculation method for the coordinates of the boundary and the radius of the crater ejecta is the same as the calculation method for the coordinates of the crater rim and the radius of the crater, and it is applicable to all samples.

IV. Experiments and Results

A. Analysis of a Single Crater

This section uses the above proposed method to analyze the study area where Crater2 is located.

Fig. 3(a) shows the m_v image of the study area. A polar coordinate system is established according to the method described above, and the number of samples is set to 360. S_{190} is the sample extracted at a sampling angle of 190°. Fig. 3(b) is the set of all samples extracted in Fig. 3(a), and the position corresponding to S_{190} is marked as a solid white line. It can be observed that m_v rapidly increases in the direction of the ejecta flow and gradually decreases until it is smooth. The accumulation in the hot area of the crater rim is most obvious. The influence of different local incident angles makes the accumulation of the hot area nonuniform.

Fig. 4 shows the m_v data of S_{190} and the data after mean filtering. The m_v curve in Fig. 4 does not completely conform to the rules shown in Fig. 2(a) since there are some smaller craters within the range of the crater ejecta as shown in Fig. 3(a), which makes fluctuations marked Q1, Q2, and Q3 as shown in Fig. 4.

To extract the crater rim, the radial distance is limited within twice the radius of the crater as shown in Fig. 5. According to (4), the fitting result is

$$f_c(r) = 0.1244 \times \exp\left(-\left(\frac{r - 578.3}{170.8}\right)^2\right) + 0.04641 \times \exp\left(-\left(\frac{r - 721.6}{946.4}\right)^2\right) \tag{10}$$

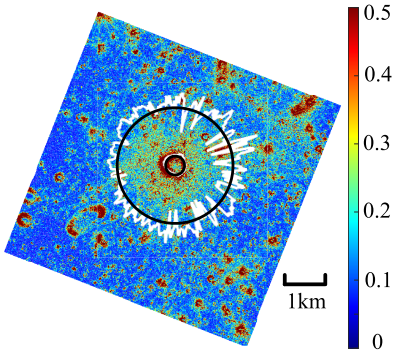

Fig. 7. Characterization results of the range of the crater ejecta. The white lines are the results presented using samples. The black concentric circles are the result of fitting all results.

TABLE II
Radius of Crater of All Study Areas

Index	Name	R_c/km	R_{crater}/km	Accuracy
1	Crater1	0.5076	0.50	0.98
2	Crater2	0.6853	0.70	0.98
3	Lassell D	1.1747	1.05	0.88
4	Linne	1.2072	1.20	0.99
5	Herigonius K	1.3674	1.45	0.94
6	La Condamine S	2.1964	1.95	0.87

where $0 \le r \le 1400$. It can be obtained that the maximum value of m_v in the interval is 0.1708 through (10), and $r = 578.3$. Therefore, it can be known that the distance from the crater rim to the first sample point is 578.3 m in S_{190}.

By performing statistics on all the data in S_{190} with (7), (8), it can be known that 0.0168 represents the lunar background level of m_v in S_{190}, which can also be used as a threshold to distinguish between the two regions in the curve fitting of the crater ejecta and the lunar background regolith.

Extracting all data after the crater rim in S_{190} and beginning extracting the boundary between the crater ejecta and the lunar background regolith, the data distribution is shown in Fig. 6. The suppression results of abnormal fluctuations in the data are shown in Q4, Q5, and Q6 in Fig. 6. The data without abnormal data are fit using (6), and the result is

$$f_e(r) = 0.2063 \times r^{-0.5808} + 0.003566 \tag{11}$$

where $r \ge 0$.

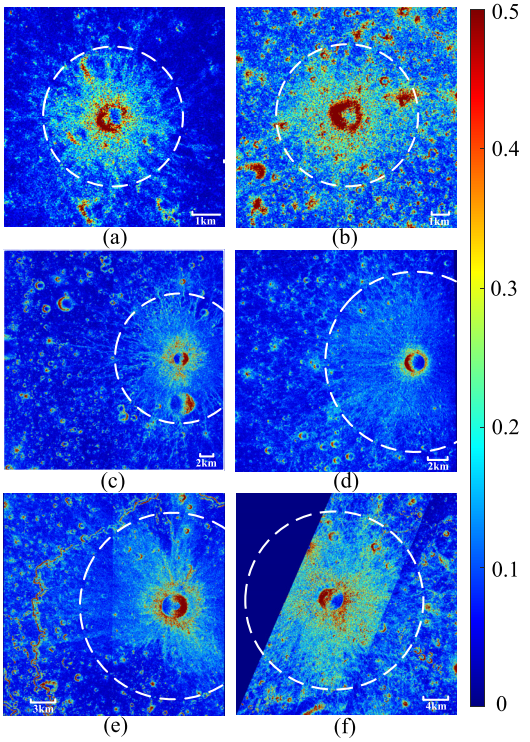

Fig. 8. Range of the crater ejecta obtained through visual interpretation. Items (a)–(f) correspond to the craters represented by numbers 1–6 in Table I.

TABLE III
RADIUS OF CRATER EJECTA OF ALL STUDY AREAS

Index	Name	R_e/km	R_{ejecta}/km	Accuracy
1	**Crater1**	2.7225	3.05	0.89
2	**Crater2**	4.1334	3.86	0.93
3	**Lassell D**	7.6527	8.62	0.89
4	**Linne**	8.1565	9.85	0.82
5	**Herigonius K**	10.0826	11.1	0.91
6	**La Condamine S**	16.7830	15.8	0.94

Combining the lunar background level of m_v obtained above and according to (9), it can be known that the distance between the boundary of the crater ejecta and the crater rim is 3349.8 m. Combining the distance from the crater rim to the first sampling point obtained above, it can be known that the distance from the boundary of crater ejecta in S_{190} to the first sampling point is 3928.2 m.

Applying the above process to all samples, the coordinates of the crater center can be calculated through the information obtained from the crater rim. Then, using the method mentioned in Section III-C, the radius of the crater can be obtained as 685.3 m and the radius of the crater ejecta is 4133.4 m. Fig. 7 shows the characterization results of the range of crater ejecta.

B. Analysis of All Study Areas

The range of the crater ejecta of all study areas obtained through visual interpretation is shown in Fig. 8. The specific information on the radius of the crater and the radius of the crater ejecta obtained by the method proposed in this letter are shown in Tables II and III. Among them, R_c and R_e are the radius of the craters and the radius of the ejecta, respectively, obtained through the proposed method. R_{crater} is the radius of the crater obtained through optical imagery. And R_{ejecta} is the radius of the crater ejecta obtained through visual interpretation. The experimental results validate the effectiveness of the proposed method.

V. CONCLUSION

This letter proposes a new systematic methodology to characterize the range of the simple fresh lunar crater ejecta. The component m_v representing the volume scattering process in the three-component compact decomposition is used to represent the scattering characteristics of different regions of the lunar surface. The crater rim and the boundary of the crater ejecta are extracted by analyzing the differences in the distribution of scattering mechanisms between the crater ejecta and surrounding regions and the changes in scattering characteristics. The final experimental results were compared with the range of the ejecta obtained through visual interpretation on SAR imagery, and the results showed that the proposed method can effectively distinguish between the crater ejecta and surrounding regions of the lunar surface.

REFERENCES

[1] Z. Yue, K. Shi, K. Di, Y. Lin, and S. Gou, "Progresses and prospects of impact Crater studies," *Sci. China Earth Sci.*, vol. 66, no. 11, pp. 2441–2451, Dec. 2022.
[2] H. J. Melosh, "Ejecta deposits," in *Impact Crater: A Geologic Process*, vol. 6. New York, NY, USA: Oxford Univ. Press, 1989, pp. 87–111.
[3] S. W. Bell, B. J. Thomson, M. D. Dyar, C. D. Neish, J. T. S. Cahill, and D. B. J. Bussey, "Dating small fresh lunar craters with mini-RF radar observations of ejecta blankets," *J. Geophys. Res., Planets*, vol. 117, no. E12, Nov. 2012, Art. no. E004007.
[4] S. Zang, L. Mu, L. Xian, and W. Zhang, "Semi-supervised deep learning for lunar Crater detection using CE-2 DOM," *Remote Sens.*, vol. 13, no. 14, p. 2819, Jul. 2021.
[5] M. Chen, D. Liu, K. Qian, J. Li, M. Lei, and Y. Zhou, "Lunar Crater detection based on terrain analysis and mathematical morphology methods using digital elevation models," *IEEE Trans. Geosci. Remote Sens.*, vol. 56, no. 7, pp. 3681–3692, Jul. 2018.
[6] R. K. Raney et al., "The lunar mini-RF radars: Hybrid polarimetric architecture and initial results," *Proc. IEEE*, vol. 99, no. 5, pp. 808–823, May 2011.
[7] Y. Gao et al., "Investigating the dielectric properties of lunar surface regolith fines using mini-RF SAR data," *ISPRS J. Photogramm. Remote Sens.*, vol. 197, pp. 56–70, Mar. 2023.
[8] R. K. Raney, J. T. S. Cahill, G. W. Patterson, and D. B. J. Bussey, "The m-chi decomposition of hybrid dual-polarimetric radar data with application to lunar craters," *J. Geophys. Res., Planets*, vol. 117, no. E12, Dec. 2012, Art. no. E00H21.
[9] L. M. Carter et al., "Initial observations of lunar impact melts and ejecta flows with the Mini-RF radar," *J. Geophys. Res., Planets*, vol. 117, no. E12, Feb. 2012, Art. no. E00H09.
[10] S. R. Cloude, D. G. Goodenough, and H. Chen, "Compact decomposition theory," *IEEE Geosci. Remote Sens. Lett.*, vol. 9, no. 1, pp. 28–32, Jan. 2012.
[11] J. Laura et al., "Integrated software for imagers and spectrometers (7.2.0_RC1)," *Zenodo*, 2023, doi: 10.5281/zenodo.7644616.
[12] W. Fa, M. A. Wieczorek, and E. Heggy, "Modeling polarimetric radar scattering from the lunar surface: Study on the effect of physical properties of the regolith layer," *J. Geophys. Res.*, vol. 116, no. E3, Mar. 2011, Art. no. E03005.
[13] A. M. Stickle, G. W. Patterson, J. T. S. Cahill, and D. B. J. Bussey, "Mini-RF and LROC observations of mare Crater layering relationships," *Icarus*, vol. 273, pp. 224–236, Jul. 2016.